Photocatalytic properties of KBiO$_3$ and LiBiO$_3$ with tunnel structures

RAJALAKSHMI RAMACHANDRAN[c], M SATHIYA[a], K RAMESHA[a], A S PRAKASH[a], GIRIDHAR MADRAS[b,c] and A K SHUKLA[b,*]

[a]CSIR-Central Electrochemical Research Institute-Madras Unit, CSIR-Madras Complex, Taramani, Chennai 600 113, India
[b]Solid State and Structural Chemistry Unit, [c]Department of Chemical Engineering, Indian Institute of Science, Bangalore 560 012, India
e-mail: akshukla2006@gmail.com

Abstract. In the present study, KBiO$_3$ is synthesized by a standard oxidation technique while LiBiO$_3$ is prepared by hydrothermal method. The synthesized catalysts are characterized by X-ray diffraction (XRD), Scanning Electron Microscopy (SEM), BET surface area analysis and Diffuse Reflectance Spectroscopy (DRS). The XRD patterns suggest that KBiO$_3$ crystallizes in the cubic structure while LiBiO$_3$ crystallizes in orthorhombic structure and both of these adopt the tunnel structure. The SEM images reveal micron size polyhedral shaped KBiO$_3$ particles and rod-like or prismatic shape particles for LiBiO$_3$. The band gap is calculated from the diffuse reflectance spectrum and is found to be 2.1 eV and 1.8 eV for KBiO$_3$ and LiBiO$_3$, respectively. The band gap and the crystal structure data suggest that these materials can be used as photocatalysts. The photocatalytic activity of KBiO$_3$ and LiBiO$_3$ are evaluated for the degradation of anionic and cationic dyes, respectively, under UV and solar radiations.

Keywords. KBiO$_3$; LiBiO$_3$; synthesis; crystal structure; photocatalysis.

1. Introduction

Dyes find multifarious applications including textile, paper, and plastic industries. The release of dye effluents without proper treatment is environmentally deleterious. Accordingly, there is a definite necessity for degrading the dyes such that the final discharge contains permissible limits of effluents. There are several treatment methods and each has its own merits and demerits.[1,2] However, the advanced oxidation processes (AOPs) happen to be among the most promising treatment methods. AOPs involve the formation of hydroxyl radicals as powerful chemical oxidant. Among the various AOPs, photocatalysis is considered to be the most efficient and popular remediation process.[3–6] In photocatalysis, when the light energy is greater than or equal to the band gap of semiconductor, the electron-hole pairs are generated and the hydroxyl and superoxide radicals are produced which help in oxidizing the organic pollutants.[7]

TiO$_2$ is the most widely used photocatalytic material. It has many advantages over the other semiconductors such as high stability, resistance to photo corrosion, low toxicity and low cost.[8–10] However, the wide band gap of the TiO$_2$ ($\sim$ 3.2 eV) limits its usage under visible light. To overcome this issue, studies are being conducted to develop newer materials.[10,11] Bismuth-based compounds such as BiVO$_4$, Bi$_2$WO$_6$, Bi$_2$MoO$_6$, CaBi$_2$O$_4$, BiNbO$_4$ and BiTaO$_4$ have been reported as new photocatalytic materials.[12–20] Many Bi^{+3} containing oxides exhibit photocatalytic properties due to the hybridized O(2p) and Bi (6s) valence bands. Recently, BaBiO$_3$ a perovskite oxide, where Bi present in +3 and +5 mixed oxidation states, has been shown to be an active visible-light-driven photocatalyst.[21] Theoretical calculations have shown that both the valence band (VB) and the conduction band (CB) of BaBiO$_3$ comprise hybridized orbitals. The higher activity of BaBiO$_3$ for both acetaldehyde decomposition and methylene blue (MB) degradation has been attributed to its special band structure that facilitates transfer of photoelectrons from 6s orbitals of Bi^{+3} to the 6s orbitals of Bi^{+5}. Apart from Bi (III) containing compounds, Bi (V) containing compounds have also been reported as active photocatalysts.[22–26] NaBiO$_3$ exhibits much higher activity compared to BiVO$_4$ and n-doped TiO$_2$ for the decomposition of methylene blue (MB) under visible light. The attractive performance of NaBiO$_3$ is ascribed to its band

structure where the CB consists of hybridized Na (3s) and O (2p) orbitals that exhibit large dispersion with high mobility for photo-excited electrons.

KBiO$_3$[27,28] and LiBiO$_3$[29] are two other compounds containing Bi^{+5}. NaBiO$_3$ has Ilmenite structure,[30] while KBiO$_3$ and LiBiO$_3$ exhibit tunnel structures[31] akin to KSbO$_3$. Nevertheless, there are similarities between Ilmenite and tunnel structure, as both are formed by edge-sharing octahedra. Accordingly, KBiO$_3$ and LiBiO$_3$ are also expected to exhibit photocatalytic behaviour similar to NaBiO$_3$. In this study, we report the synthesis and photocatalytic properties of KBiO$_3$ and LiBiO$_3$.

2. Experimental

2.1 *Materials*

The dyes, orange G (OG), amido black 10B (AB10B), rhodamine B (RhB) and methylene blue (MB) were from S.D.Fine-Chem Ltd., India, alizarin cyanine green (ACG) and indigo carmine (IC) were from Rolex Chemical Industries, India and coomassie brilliant blue R 250 (CBBr) was from Merck Ltd., India. Milli-Q water was used for all the experiments. The structure of the various dyes used in the present study is given in the figure 1.
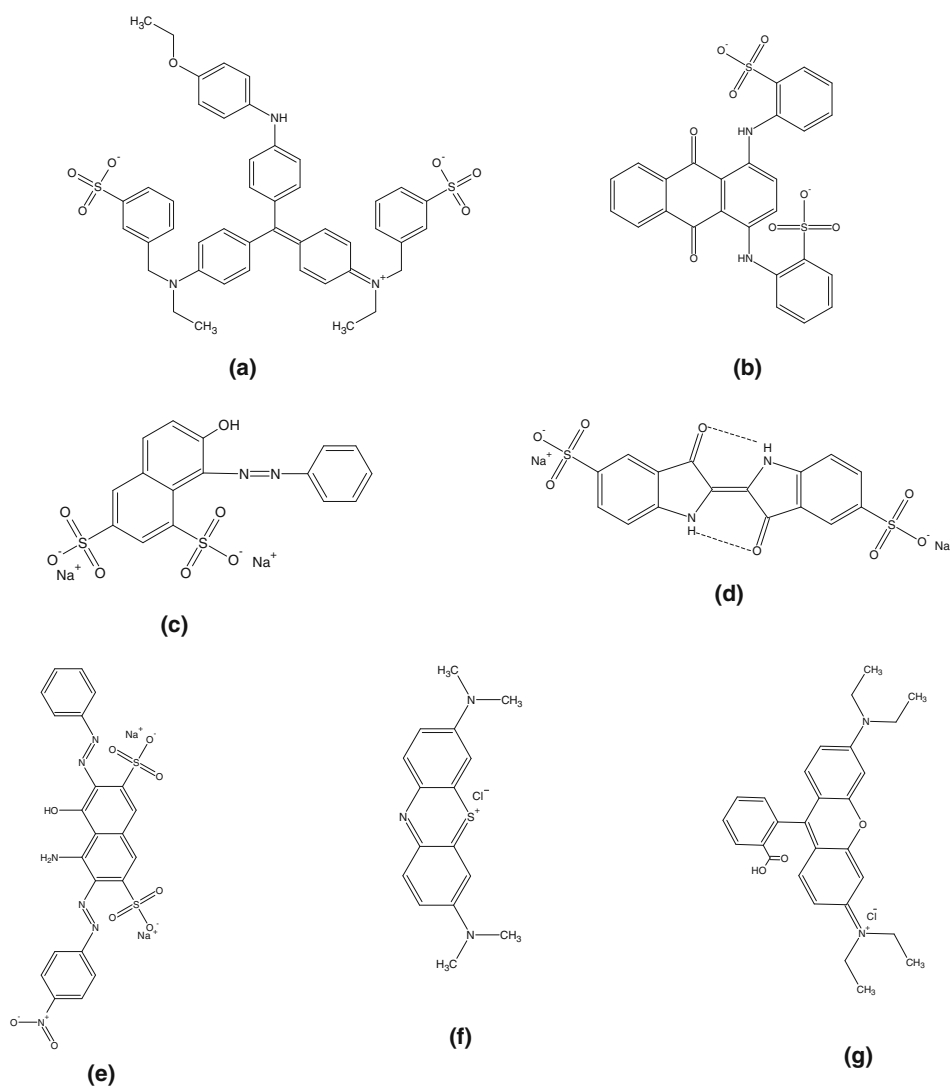
Figure 1. Structure of various dyes used in the study. (**a**) Coomassie brilliant blue R 250 (CBBr), (**b**) alizarin cyanine green (ACG), (**c**) orange G (OG), (**d**) indigo carmine (IC), (**e**) amido black 10B (AB10B), (**f**) methylene blue (MB), and (**g**) rhodamine B (RhB).

2.2 *Synthesis*

KBiO$_3$ was prepared according to the method reported by Brauer.[32] KBiO$_3$ was synthesized by the oxidation of 3.3 g of Bi$_2$O$_3$ in 30 ml of 50% aqueous KOH by 4 ml of Br$_2$ at the boiling point. The bright red precipitate of KBiO$_3$ so formed was filtered and washed with 40% KOH and cold water. LiBiO$_3$ was prepared by hydrothermal method.[29] The starting materials, NaBiO$_3$. 2H$_2$O and LiOH, were placed in a Teflon lined autoclave (70 ml) with Li/Bi molar ratio of 4. The autoclave with 50% water filling was heated at 120°C for 2 days. The brown product obtained was filtered and washed with water several times and dried.

2.3 *Characterization*

The powder X-ray diffraction data (XRD) were obtained on a Philips (Xpert PRO) machine using CuK$_\alpha$ source. The XRD patterns were matched with the related JCPDS pattern using X'Pert HighScore plus software program.[33] The morphology and particle size were analysed using scanning electron microscope (JEOL-JSM-5600LV, 20 kV). The surface area of powder samples were determined by nitrogen adsorption BET technique (Belsorp, Japan). The UV-visible diffuse reflectance spectra (DRS) for the powder samples were recorded using UV-Visible spectrometer (Lambda 32, PerkinElmer). The K and Li contents in KBiO$_3$ and LiBiO$_3$ samples were obtained using a Perkin-Elmer Atomic Absorption Spectrometer.

2.4 *Photocatalytic degradation*

The photoreactor comprised of a jacketed quartz tube (3.8 cm i.d., 4.5 cm o.d. and 21 cm length) and a Pyrex reactor (5.2 cm i.d. and 16 cm length). The high pressure mercury vapor lamp (125 W) was placed inside the quartz tube and 100 ml of the dye solution was taken in the Pyrex reactor. Both the quartz tube and Pyrex reactor were cooled by the circulation of water to maintain the temperature of the dye solution at 25°C.

The degradation experiments were carried out under UV radiation with initial concentration of 50 mg/l for OG, IC, AB10B, ACG, RhB, 15 mg/l (CBBr) and 20 mg/l (MB) and the catalyst loading was kept at 1 g/l for all the experiments. Prior to the photocatalysis, the suspension was left in dark for 2 h for the attainment of adsorption–desorption equilibrium. The samples were collected in vials at regular intervals of time and centrifuged so as to remove the catalyst.

The degradation experiments were also carried out under solar radiation. All the solar experiments were carried out in a crystallizing dish having inner diameter of 100 mm and a height of 50 mm with same initial concentrations of dyes and the catalyst loadings as for UV radiation experiments. In brief, 50 ml of dye solution along with the catalyst was taken in the crystallizing dish. The solution was then exposed to sunlight with a perfectly transparent glass plate to cover the top to ensure high solar exposure while ensuring little evaporation. The intensity of the solar radiation was measured on all experimental days so as to ensure that the reactions were carried out under similar conditions. The average solar intensity was ∼ 975 W/m^2. The solution was stirred continuously for two hours during the degradation. Samples were taken at regular intervals, centrifuged to remove the catalyst and analysed by UV spectrophotometer.

The samples were analysed and the decrease in absorbance of the dye solution at the characteristic wavelength over the entire period of time was monitored on a Shimadzu 1700 UV-vis spectrometer. The absorbance corresponding to the λ_{max} were converted to the concentration using the predetermined calibration curves for each dye.

3. **Results and discussion**

3.1 *Characterization of the catalysts*

Figure 2 shows the XRD patterns for KBiO$_3$ and LiBiO$_3$ samples that match well with the reported patterns for KBiO$_3$ (ICDD PDF Card No.00–047–0879) and LiBiO$_3$ (ICDD PDF Card No. 01–086–1187). Lattice parameters obtained are close to the reported values for these oxides. KBiO$_3$ crystallizes in cubic KSbO$_3$ type structure (space group $Im\bar{3}$) with lattice parameter $a = 10.0198(3)$ Å. LiBiO$_3$ has orthorhombic structure (space group $Pccn$) similar to LiSbO$_3$ and the lattice parameters obtained are: $a = 8.8272(2)$, $b = 4.9138(2)$, and $c = 10.6919(3)$ Å. The structures of KBiO$_3$ and LiBiO$_3$ are based on pairs of edge-shared BiO$_6$ octahedra to form Bi$_2$O$_{10}$ clusters. These clusters share corners to form tunnel structures, as shown in figure 3. Alkali ions are located in the tunnels. More details about the crystal structures of KBiO$_3$/LiBiO$_3$ could be found elsewhere.[29,31] The adoption of a tunnel structure by KBiO$_3$ and LiBiO$_3$ ascribed to a large covalency of Bi–O bonds. Goodenough and Kafalas have argued that in the absence of Bi–O π–bonding interactions, strong covalency favours edge sharing and inhibit linear Bi–O–Bi bonds.[31,34]
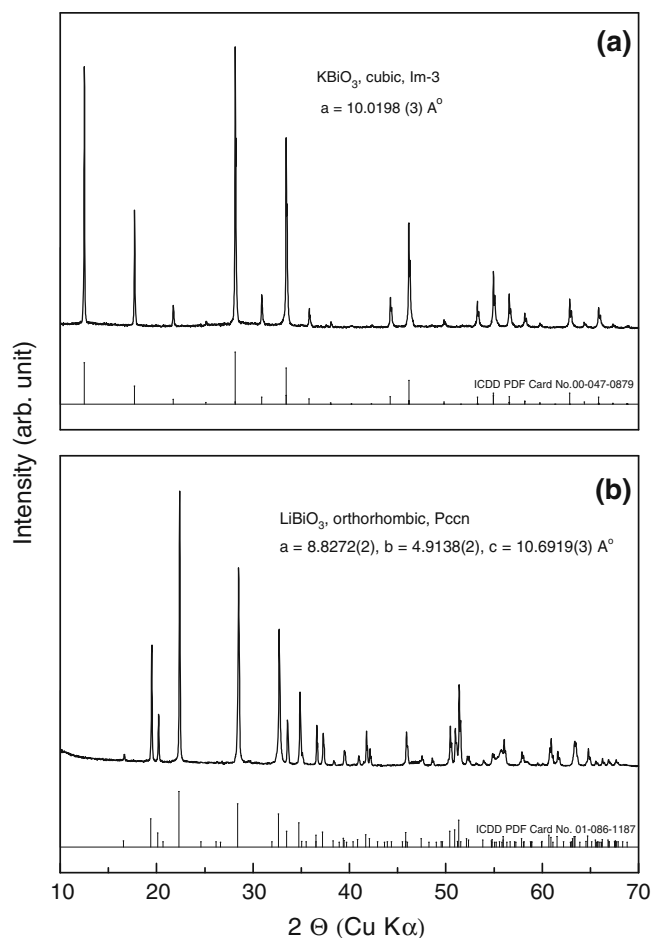
Figure 2. XRD patterns of (**a**) KBiO$_3$ and (**b**) LiBiO$_3$.

The scanning electron micrographs for KBiO$_3$ and LiBiO$_3$ samples taken at higher magnifications are shown in figure 4. It is clearly seen from the micrographs that the particle morphology depends on the

method of synthesis. As seen in the micrograph (figure 4a), KBiO$_3$ phase comprises micron size particles having polyhedral appearance. For LiBiO$_3$, two distinct particle morphologies, namely rod-like or prismatic particles, are observed. The surface areas for the catalysts were found to be $\sim 1\,m^2/g$. The K and Li content in KBiO$_3$ and LiBiO$_3$ samples, estimated from Atomic Absorption Spectroscopy, are found to be close to the nominal stoichiometry.

UV-vis diffused-reflectance spectra (DRS) for KBiO$_3$ and LiBiO$_3$ powder samples are shown in figure 5. The band gap (E$_g$) from UV-vis diffused-reflectance spectra (DRS) of powder samples is estimated by plotting first derivative of absorbance with respect to photon energy (eV) and finding the maxima in the derivative spectra at the lower energy side. The maximum in the derivative spectra, i.e., where the absorbance has a maximum increase with respect to photon energy, is assigned as E$_g$. Accordingly, the calculated band gaps from absorption spectra for KBiO$_3$ and LiBiO$_3$ are estimated to be 2.1 eV and 1.8 eV, respectively. The absorption spectra are consistent with the colours of the compounds; KBiO$_3$ is bright red while LiBiO$_3$ is brown indicating considerable visible light absorption by these oxides. In Bi-oxides the chemical nature of spectator cation (Li$^+$, K$^+$, Na$^+$, Ag$^+$, Ba^{+2}) plays an important role in tailoring the band structure[35,36] as also in stabilizing different oxidation states ($+3$ to $+5$) for Bi.

3.2 *Photocatalytic degradation*

The photolysis was carried out for all the dyes to ensure that there is negligible effect with the lamp alone. Accordingly, the decrease in the concentration of dye is
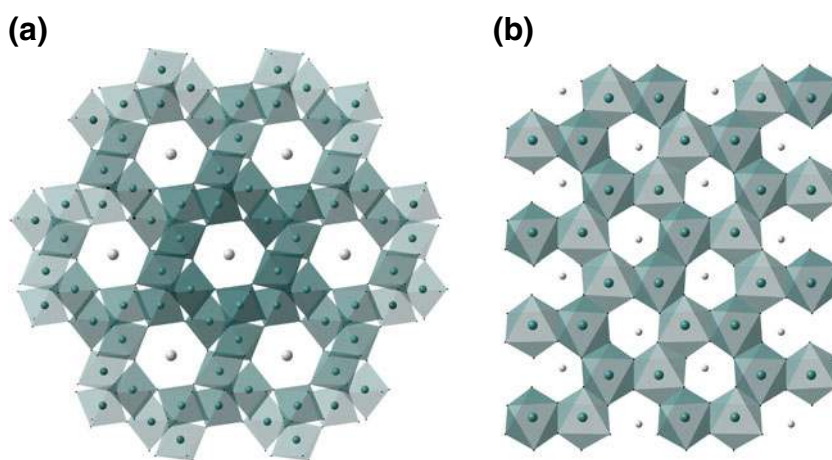
Figure 3. Crystal structure of (**a**) KBiO$_3$ and (**b**) LiBiO$_3$. Oxygen atoms are at the corner of the octahedron around Bi^{+5} while K$^+$/Li$^+$ cations reside within the tunnels.
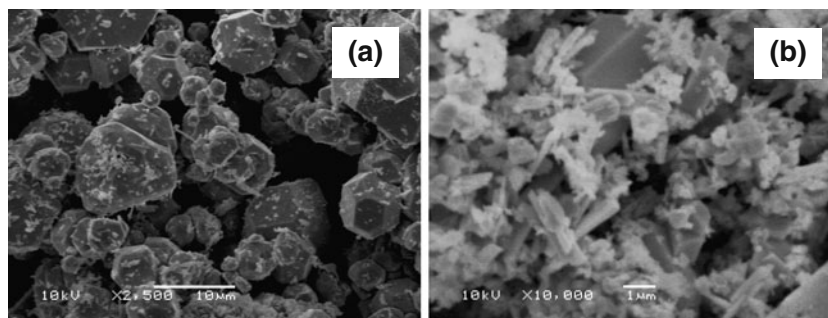
Figure 4. SEM images for (**a**) KBiO₃ and (**b**) LiBiO₃.
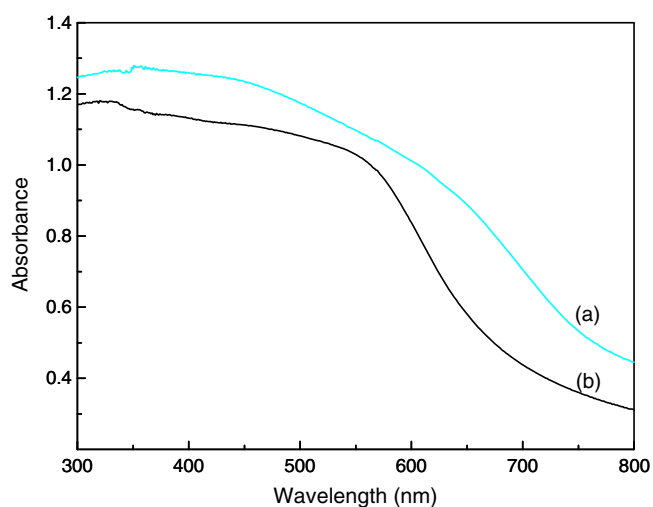
Figure 5. Diffuse reflectance spectra for (**a**) LiBiO₃ and (**b**) KBiO₃.

due to the effect of both the catalyst and the UV light. The concentration of the dye after the 2 h of adsorption is taken as the initial concentration (C_0). LiBiO₃ shows a significant adsorption of anionic dyes while cationic dyes are adsorbed significantly on KBiO₃. The adsorption of the dye on a material is due to the surface charge of the material and the ionic state of the dyes, and is independent of the size of the dye and surface area of the material. Accordingly, the difference in the adsorption of the dyes can be attributed to the difference of the surface charge on the catalysts. The negatively charged sulfonic acid groups of the anionic dyes are attracted to the positively charged LiBiO₃. Due to the strong adsorption, photocatalysis could not be investigated for the anionic dyes on LiBiO₃ and the cationic dyes on KBiO₃. Therefore, photocatalytic degradation of anionic and cationic dyes is carried out in presence of KBiO₃ and LiBiO₃, respectively.

KBiO₃ was used to carry out the photocatalytic degradation of the anionic dyes of five classes, namely mono-azoic (OG), di-azoic (AB10B), anthroquinonic

(ACG), Indigo (IC) and triaryl methane (CBBr). Figures 6a and b show the degradation profiles, i.e., normalized concentration (C/C_0) with time, for the degradation of anionic dyes with KBiO₃ under UV and
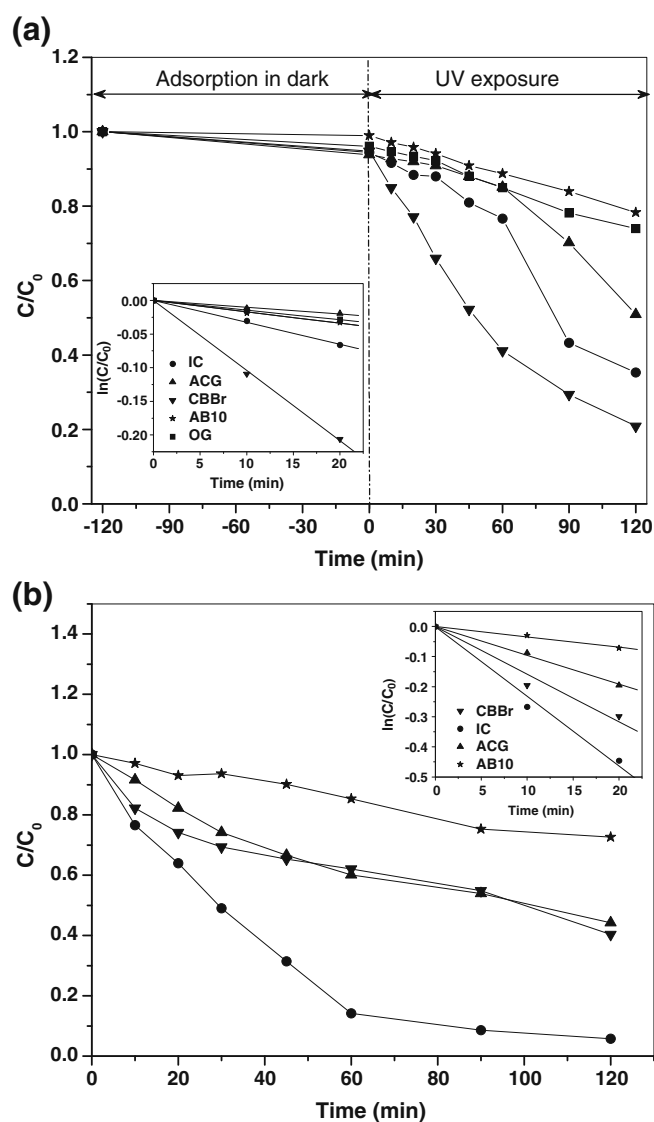
Figure 6. Degradation profiles of anionic dyes with KBiO₃ under (**a**) UV and (**b**) solar radiation.

(a)

(b)
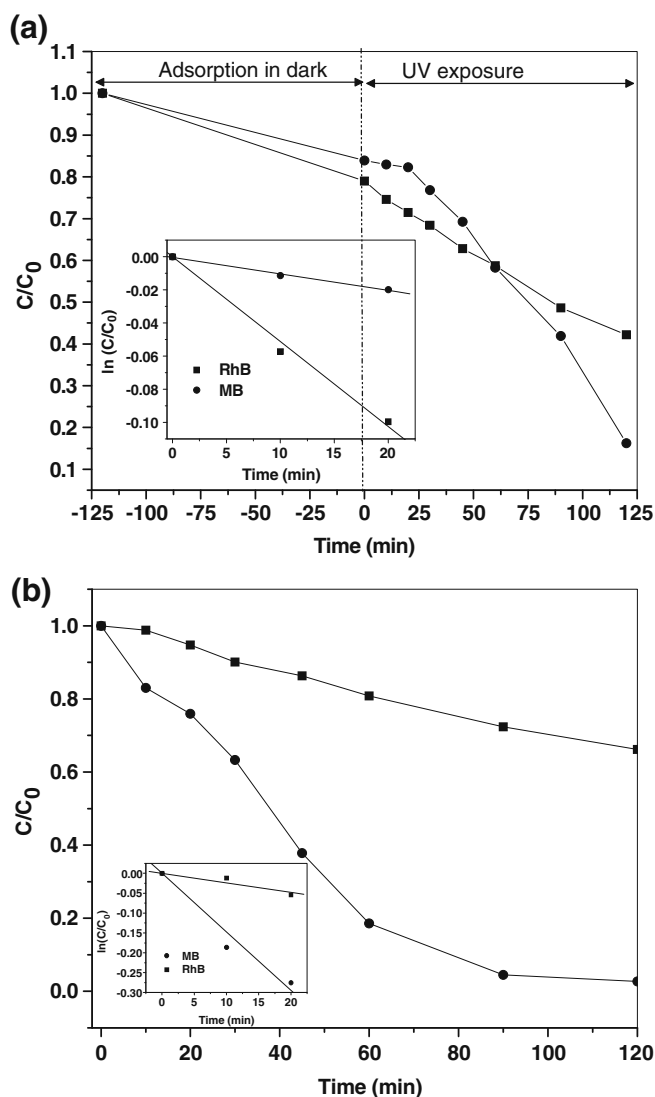
Figure 7. Degradation profiles of cationic dyes with LiBiO$_3$ under (**a**) UV and (**b**) solar radiation.

solar radiations, respectively. The photocatalytic activity of LiBiO$_3$ is evaluated by carrying out degradation of two cationic dyes, RhB (Xanthene fluorine rhodamine) and MB (Quinone imine thiazine). Figures 7a and b show the variation in normalized concentration with time for MB and RhB in presence of LiBiO$_3$ under UV and solar radiations, respectively. The initial degradation of the dyes is found to follow the first order kinetics for both the UV and solar radiations. The initial rate constants are determined from the slope of ln (C/C$_0$) with time as shown in the inset to figures 6a, b, 7a and b. The rate constants and the initial rates are given in table 1. The initial rates are found to be higher for solar radiation than that for the UV radiation but a direct comparison could not be made because the intensities happen to be different.

The degradation of the dye can be attributed to the catalytic effect, which results in the generation of charge carriers, namely the valence band holes and conduction band electrons, when the materials are irradiated by UV or solar light. The holes and electrons participate in the photocatalysis pathway generating hydroxyl (OH·) radicals, which are the precursors for decomposition of any organic substrate. These hydroxyl species oxidize the dye through the formation of intermediates, which on prolonged exposure to UV mineralize the dye to smaller fragments like carbon dioxide, water and other inorganic ions.

The initial rate constant, k, calculated from the slope of ln (C/C$_0$) versus time (inset of figure 6a, table 1), for the degradation of dyes follows the trend ACG < OG < AB10B < IC < CBBr. However, because the initial concentration of the dyes are different, the initial rates (table 1) are calculated based on k C$_0$, follow the trend ACG < OG < AB10B < CBBr < IC. The same trend was observed for the degradation of dyes with DP-25 TiO$_2$, as reported by Vinu *et al.*[37] However, the

Table 1. Rate constants for the photocatalytic degradation of various dyes.

Dyes	Class	Under UV radiation		Under solar radiation	
		Rate constants k (min^{-1})	Initial rate r$_0$ (mg L^{-1} min^{-1})	Rate constants k (min^{-1})	Initial rate r$_0$ (mg L^{-1} min^{-1})
KBiO$_3$					
IC	Indigo	0.00326	0.15399	0.02319	1.15950
CBBr	Triaryl methane	0.01043	0.14827	0.01585	0.23775
AB10B	Diazoic	0.00170	0.08416	0.00345	0.1725
OG	Monoazoic	0.00144	0.0692	0.0	0.0
ACG	Anthraquinonic	0.00102	0.04785	0.00958	0.47900
LiBiO$_3$					
RhB	Xanthene Fluorene Rhodamine	0.00513	0.20255	0.00240	0.12000
MB	Quinone imine Thiazin	0.00102	0.01712	0.01473	0.29460

overall degradation at the end of 2 h follows a trend: AB10B ≈ OG < ACG < IC < CBBr under UV exposure (figure 6a). Under solar radiation the overall degradation and the initial rate constant follows the trend: IC > CBBr > ACG > AB10B while the initial rate follows the trend: IC > ACG > CBBr > AB10B (figure 6b). The structure of the dye plays a crucial role as it determines the effectiveness with which the photocatalytic material can attack the functional groups in order to disrupt the aromatic ring of the dye. Therefore, the rate of degradation of the dye is very much dependent on the structure of the dye. We now attempt to explain the trend observed in this study for the rates of degradation of various dyes.

The initial rates are higher for the degradation of IC both under UV and solar radiation. A thorough study on the photocatalytic degradation of IC and their intermediates by Vautier *et al.*[38] suggests that the C–S bond cleavage is observed as the initial step during the degradation of IC followed by the formation of nitrate and ammonium ions. The central –C=C– bond has been found to be very reactive and favours the rapid degradation of the IC. In polar solvents, such as water, the intermolecular hydrogen bonds in the solvent disrupt the planarity[37] and result in the cleavage of the central –C=C– bond. This leads to the rapid degradation of IC, both under UV and solar radiation.

The overall degradation of CBBr and ACG are higher than that of OG and AB10B. Sulfonate ions play a major role in the photodegradation of dyes. The ease of generation of these ions primarily depends on the location of the sulfonyl group in the dye molecule.[39] Sulfonyl group is attached to the benzene ring in CBBr and ACG which makes it more reactive, whereas it is attached to the less reactive naphthalene in the case of OG and AB10B.

AB10B, a diazo dye, shows a higher initial rate than that of monazo dye OG. During the degradation of the azodye, the –N=N– bond breaks.[37] Ammonium ions are formed in AB10B having a primary amine group, which over a period of time forms the nitrate ions. AB10B has two azo groups, an amino group and a nitro group, which is highly reactive, and, therefore, degrade faster than OG, which contains only one azo group. OG does not undergo significant degradation under solar radiation, which might be due to its lower characteristic wavelength (λ_{max} = 480 nm), when compared to the other dyes. Therefore, the amount of electron hole pairs generated on solar exposure, which has a characteristic peak at 550 nm, will be smaller. Accordingly, this leads to lower degradation rate of OG compared to other dyes, especially under solar radiation.

In case of the degradation of the cationic dyes, the overall degradation of the methylene blue is higher than Rhodamine B under both UV and solar radiations. The presence of two dimethylamino group in MB results in the generation of methyl radicals which further oxidize during the reaction.[39] In case of the degradation of Rhodamine B, de-ethylation is followed by further reactions. Since the primary step in the degradation of the dyes are different and the rate of de-ethylation is slower than the generation of the methyl radicals, the overall degradation of methylene blue is higher than that for the degradation of Rhodamine B, both under UV and solar radiation.

4. Conclusions

In this study, the catalyst KBiO₃ and LiBiO₃ were synthesized and characterized by XRD, SEM and diffuse reflectance spectroscopy. Unlike the NaBiO₃, which has Ilmenite structure, these compounds possess the tunnel structure. The diffuse reflectance spectroscopy showed that the catalysts have a broad absorbance around 600 nm with band gap of ∼ 2 eV. Due to the low band gap, the catalysts were tested for the photocatalytic activity under solar light and UV light exposure. The photocatalytic studies were carried out for the degradation of anionic dyes and cationic dyes with KBiO₃ and LiBiO₃ respectively.

References

1. Crini G 2006 *Bioresour. Technol.* **97** 1061
2. Robinson T, McMullan G, Marchant R and Nigam P 2001 *Bioresour. Technol.* **77** 247
3. Rajeshwara K, Osugib M E, Chanmaneec W, Chenthamarakshana C R, Zanonib M V B, Kajitvichyanukuld P and Krishnan-Ayera R 2008 *J. Photochem. Photobiol. C: Photochem. Rev.* **9** 171
4. Hoffmann M R, Martin S T, Choi W and Bahemann D W 1995 *Chem. Rev.* **95** 69
5. Teichner S J 2008 *J. Porous Mater.* **15** 311
6. Robertson P K J 1996 *J. Cleaner Prod.* **4** 203
7. Mills A, Hill G, Crow M and Hodgen S 2005 *J. Appl. Electrochem.* **35** 641
8. Akpan U G and Hameed B H 2009 *J. Hazard. Matter.* **170** 520
9. Kitano M, Matsuoka M, Ueshima M and Anpo M 2007 *Appl. Catal. A* **325** 1
10. Zhu J and Zach M 2009 *Current opinion in Colloid and Interface Science* **14** 260
11. Hernandez-Alonso M D, Fresno F, Suarez S and Coronado J M 2009 *Energy Environ. Sci.* **2** 1231
12. Kudo A, Omori K and Kato H 1999 *J. Am. Chem. Soc.* **121** 11459

13. Tokunaga S, Kato H and Kudo A 2001 *Chem. Mater.* **13** 4624
14. Zhang A, Zhang J, Cui N, Tie X, An Y and Li L 2009 *J. Mol. Catal A: Chem.* **304** 28
15. Zhou Y, Vuille K, Heel A, Probst B, Kontic R and Patzke G R 2010 *Appl. Catal. A* **375** 140
16. Guo Y, Yang X, Ma F, Li K, Xu L, Yuan X and Guo Y 2010 *Appl. Surf. Sci.* **256** 2215
17. Ren J, Wan W, Zhang L, Chang J and Hu S 2009 *Catal. Commun.* **10** 1940
18. Zheng Y, Duan F, Wu J, Liu L, Chen M and Xie Y 2009 *J. Mol. Catal. A: Chem.* **303** 9
19. Tang J, Zou Z and Ye J 2004 *Angew. Chem. Int. Ed.* **43** 4463
20. Muktha B, Darriet J, Madras G and Guru Row T N 2006 *J. Solid State Chem.* **179** 3919
21. Tang J, Zou Z and Ye J 2007 *J. Phys. Chem. C* **111** 12779
22. Kako T, Zou Z, Katagiri M and Ye J 2007 *Chem. Mater.* **19** 198
23. Chang X, Ji G, Sui Q, Huang J and Yu G 2009 *J. Hazard. Mater.* **166** 728
24. Yu K, Yang S, He H, Sun C, Gu C, and Ju Y 2009 *J. Phys. Chem. A* **113** 10024
25. Chang X, Huang J, Cheng C, Shad W, Li X, Ji G, Deng S and Yu G 2010 *J. Hazard. Mater.* **173** 765
26. Kikugawa N, Yang L, Matsumoto T and Ye J 2010 *J. Mater. Res.* **25** 177
27. Kodialam S, Korthius V C, Hoffmann R D and Sleight A W 1992 *Mater. Res. Bull.* **27** 1379
28. Nguyen T N, Giaquinta D M, Davis W M and Zur Loye H –C 1993 *Chem. Mater.* **5** 1273
29. Kumada N, Takahashi N, Kinomura N and Sleight A W 1996 *J. Solid State Chem.* **126** 121
30. Kumada N, Kinomura N and Sleight A W 2000 *Mater. Res. Bull.* **35** 2397
31. Hong H Y-P, Kafalas J A and Goodenough J B 1974 *J. Solid State Chem.* **9** 345
32. Brauer G 1965 *Handbook of preparative inorganic chemistry* (New York: Academic Press) **1** 628
33. X'Pert HighScore Plus (Version 2.2.2), PANalytical software for phase identification (Netherlands: Almelo) 2006
34. Goodenough J B and Kafalas J A 1973 *J. Solid State Chem.* **6** 493
35. Sleight A W 2009 *Prog. Solid State Chem.* **37** 251
36. Sharma R, Mandal T K, Ramesha K and Gopalakrishnan J 2004 *Indian J. Chem.* **43A** 11
37. Vinu R, Akki S U and Madras G 2010 *J. Hazard. Mater.* **176** 765
38. Vautier C M, Guillard C and Herrmann J M 2004 *J. Catal.* **201** 46
39. Lachheb H, Puzenat E, Houas A, Ksibi M, Elaloui E, Guillard C and Herrmann J M 2002 *J. Appl. Catal. B* **39** 75